Submitted to the
32nd International Conference on High Energy Physics
August 16 - 22, 2004, Beijing, China

Abstract: 5-0271 **Session: QCD hard interactions**

Study of color dynamics in photoproduction at HERA

ZEUS Collaboration

Abstract

Differential cross sections for jets produced in the photoproduction regime have been measured with the ZEUS detector at HERA using an integrated luminosity of 127 pb^{-1}. Jets were identified using the k_T cluster algorithm in the longitudinally invariant inclusive mode. Measurements of differential cross sections are presented as a function of jet angular variables to highlight the presence of a triple-gluon vertex. QCD calculations were compared to the results and used to study the underlying gauge group symmetry.

1 Introduction

Quantum chromodynamics (QCD), the gauge theory of the strong interactions which acts on the quark-fermion fields, is based on the SU(3) non-abelian group, which induces the self-coupling of the gauge bosons, the gluons. Investigations of the triple-gluon vertex have been carried out at LEP [1, 2] using angular correlations in four-jet events from Z^0 hadronic decays.

At HERA, the effects of the different color configurations arising from the underlying gauge structure should manifest itself in three-jet events in photoproduction. Photoproduction at HERA is studied by means of ep scattering at low four-momentum transfers ($Q^2 \approx 0$, where Q^2 is the virtuality of the exchanged photon). In photon-proton reactions, two types of QCD processes contribute to jet production at leading order (LO) [3, 4]: either the photon interacts directly with a parton in the proton (the direct process) or the photon acts as a source of partons which scatter off those in the proton (the resolved process). Direct-photon events provide a clean way to study the effects of the different color configurations. An illustrative diagram for each color configuration is shown in Fig. 1: (A) double-gluon bremsstrahlung from a quark line, (B) the splitting of a virtual gluon into a pair of final-state gluons, (C) the production of a $q\bar{q}$ pair through the exchange of a virtual gluon emitted by an incoming quark and (D) the production of a $q\bar{q}$ pair through the exchange of a virtual gluon arising from the splitting of an incoming gluon. Some of the variables that have been devised to highlight the contributions from the different color configurations are:

- θ_H, the angle between the plane determined by the highest transverse energy jet and the beam and the plane determined by the two lowest transverse energy jets [5];
- α_{23}, which is inspired by the variable $\alpha_{34}^{e^+e^-}$ [2] for $e^+e^- \rightarrow 4$ jets, is defined as the angle between the two lowest transverse energy jets;
- $\beta_{\rm KSW}$, which is inspired by the Körner-Schierholz-Willrodt angle $\Phi_{\rm KSW}^{e^+e^-}$ [6] for $e^+e^- \rightarrow$ 4 jets, is defined as $\cos(\beta_{\rm KSW}) = \cos\left[\frac{1}{2}\left(\angle[(\vec{p}_1 \times \vec{p}_3), (\vec{p}_2 \times \vec{p}_B)] + \angle[(\vec{p}_1 \times \vec{p}_B), (\vec{p}_2 \times \vec{p}_3)]\right)\right]$, where $\vec{p}_i,\ i = 1, ..., 3$ is the momentum of jet i and $\vec{p}_B$ is a unit vector in the direction of the beam; the jets are ordered according to decreasing transverse energy.

In e^+e^- annihilation into four-jet events, the distribution of $\Phi_{\rm KSW}^{e^+e^-}$ is sensitive to the differences between $q\bar{q}gg$ and $q\bar{q}q\bar{q}$ final states whereas that of $\alpha_{34}^{e^+e^-}$ distinguishes between contributions from double-bremsstrahlung diagrams and diagrams involving the triple-gluon coupling. In the photoproduction of three-jet events, the variable θ_H was designed to increase the sensitivity to the triple-gluon coupling in quark-induced processes (see Fig. 1B).

Differential three-jet cross sections have been measured previously in photoproduction [7]. The shape of the measured cross sections was well reproduced by perturbative QCD calculations. In this paper, measurements of the angular distributions sensitive to the contributions from the different color configurations are presented and compared to fixed-order $\mathcal{O}(\alpha\alpha_s^2)$ perturbative calculations [8].

2 Theoretical framework

The dynamics of a gauge theory such as QCD are completely defined by the commutation relations between its group generators T^i,

$$[T^i, T^j] = i \sum_k f^{ijk} \cdot T^k,$$

where f^{ijk} are the structure constants. The T^i generators can be represented as matrices. In perturbative calculations, the average and sum over all possible color configurations in the initial and final states lead to the appearance of combinatoric factors C_F, C_A and T_F, which are defined via the relations

$$\sum_{k,\eta} T^k_{\alpha\eta} T^k_{\eta\beta} = \delta_{\alpha\beta} C_F, \ \sum_{j,k} f^{jkm} f^{jkn} = \delta^{mn} C_A,$$

$$\sum_{\alpha,\beta} T^m_{\alpha\beta} T^n_{\beta\alpha} = \delta^{mn} T_F.$$

The C_F, C_A and T_F factors are known as the color factors and are the physical manifestation of the underlying group structure. In strong interactions, they represent the relative strengths of the processes $q \to qg$, $g \to gg$ and $g \to q\bar{q}$, respectively. Then, measurements of the ratios between the color factors allow the distinction between gauge groups. SU(3) predicts $C_A/C_F = 9/4$ and $T_F/C_F = 3/8$. In contrast, an abelian gluon model based on $\mathrm{U}(1)^3$ would predict $C_A/C_F = 0$ and $T_F/C_F = 3$. A non-abelian model based on SO(3) predicts $C_A/C_F = 1$ and $T_F/C_F = 1$.

The LO calculation of three-jet cross sections for direct-photon processes can be expressed in terms of the color factors C_A, C_F and T_F as follows [9]:

$$\sigma_{ep\to 3\mathrm{jets}} = C_F^2 \cdot \sigma_A + C_F C_A \cdot \sigma_B + C_F T_F \cdot \sigma_C + T_F C_A \cdot \sigma_D, \tag{1}$$

where $\sigma_A, ..., \sigma_D$ are the partonic cross sections for the different contributions (see Fig. 1).

3 Data selection and jet search

The data sample was collected with the ZEUS detector at HERA and corresponds to an integrated luminosity of 45.0 ± 0.7 (65.5 ± 1.5) pb^{-1} for e^+p collisions taken during 1995-97 (1999-2000) and 16.7 ± 0.3 pb^{-1} for e^-p collisions taken during 1998-99. During 1995-97 (1998-2000), HERA operated with protons of energy $E_p = 820$ GeV (920 GeV) and positrons or electrons[1] of energy $E_e = 27.5$ GeV, yielding a centre-of-mass energy of $\sqrt{s} = 300$ GeV (318 GeV). A detailed description of the ZEUS detector can be found elsewhere [10, 11]. A brief outline of the components that are most relevant for this analysis is given below.

Charged particles are tracked in the central tracking detector (CTD) [12], which operates in a magnetic field of 1.43 T provided by a thin superconducting solenoid. The CTD consists of 72 cylindrical drift-chamber layers, organized in nine superlayers covering the polar-angle[2] region $15^\circ < \theta < 164^\circ$. The transverse-momentum resolution for full-length tracks can be parameterised as $\sigma(p_T)/p_T = 0.0058 p_T \oplus 0.0065 \oplus 0.0014/p_T$, with p_T in GeV. The tracking system was used to measure the interaction vertex with a typical resolution along (transverse to) the beam direction of 0.4 (0.1) cm and to cross-check the energy scale of the calorimeter.

The high-resolution uranium–scintillator calorimeter (CAL) [13] covers 99.7% of the total solid angle and consists of three parts: the forward (FCAL), the barrel (BCAL) and the rear (RCAL) calorimeters. Each part is subdivided transversely into towers and longitudinally into one electromagnetic section (EMC) and either one (in RCAL) or two (in BCAL and FCAL) hadronic sections (HAC). The smallest subdivision of the calorimeter is called a cell. Under test-beam conditions, the CAL single-particle relative energy resolutions were $\sigma(E)/E = 0.18/\sqrt{E}$ for electrons and $\sigma(E)/E = 0.35/\sqrt{E}$ for hadrons, with E in GeV.

The luminosity was measured from the rate of the bremsstrahlung process $ep \rightarrow e\gamma p$. The resulting small-angle energetic photons were measured by the luminosity monitor [14], a lead-scintillator calorimeter placed in the HERA tunnel at $Z = -107$ m.

A three-level trigger system was used to select events online [11]. At the third level, a jet algorithm was applied to the CAL cells and jets were reconstructed using the energies and positions of these cells. Events with at least two jets with $E_T > 6$ GeV and $\eta < 2.5$ were accepted.

[1] Here and in the following, the term "electron" denotes generically both the electron (e^-) and the positron (e^+).

[2] The ZEUS coordinate system is a right-handed Cartesian system, with the Z axis pointing in the proton beam direction, referred to as the "forward direction", and the X axis pointing left towards the centre of HERA. The coordinate origin is at the nominal interaction point.

Events from collisions between protons and quasi-real photons were selected offline using similar criteria as reported in a previous publication [15].

The k_T cluster algorithm [16] was used in the longitudinally invariant inclusive mode [17] to reconstruct jets in the hadronic final state. The axis of the jet was defined according to the Snowmass convention [18], where $\eta^{\rm jet}$ ($\varphi^{\rm jet}$) is the transverse energy-weighted mean pseudorapidity (azimuth) of all the particles belonging to that jet. The jets were reconstructed using the CAL and were corrected for detector effects to yield jets of hadrons [15]. Events with at least three jets of transverse energy, $E_T^{\rm jet}$, above 14 GeV and $-1 < \eta^{\rm jet} < 2.5$ were retained. Direct-photon events were selected by requiring $x_\gamma^{\rm obs} > 0.7$, where $x_\gamma^{\rm obs}$, the fraction of the photon momentum participating in the production of the three jets with highest $E_T^{\rm jet}$, is defined as

$$x_\gamma^{\rm obs} = \frac{1}{2yE_e}(E_T^{\rm jet1}e^{-\eta^{\rm jet1}} + E_T^{\rm jet2}e^{-\eta^{\rm jet2}} + E_T^{\rm jet3}e^{-\eta^{\rm jet3}}),$$

where y is the inelasticity variable. The remaining contribution from resolved-photon events was estimated by Monte Carlo (MC) techniques to be $\approx$ 34%. It was checked that the angular distributions of the events from resolved processes with $x_\gamma^{\rm obs} > 0.7$ were similar to those from direct processes and, therefore, no subtraction was performed when comparing to the fixed-order calculations described in Section 5.

Neutral current deep inelastic scattering events were removed from the sample by identifying the scattered-electron candidate [19] using the pattern of energy distribution in the CAL [20]. The selected sample consisted of events from ep interactions with $Q^2 < 1$ GeV^2 and a median of $Q^2 \approx 10^{-3}$ GeV^2. The inelasticity variable y was reconstructed following the method of Jacquet-Blondel [21] from the energies measured in the CAL cells. The event sample was restricted to the kinematic range $0.2 < y < 0.85$. There remained 2233 events after all selection criteria were applied.

4 Monte Carlo simulation

The programs Pythia 6.1 [22] and Herwig 6.1 [23] were used to generate photoproduction events for resolved and direct processes. Events were generated using GRV-HO [24] for the photon and CTEQ5M1 [25] for the proton PDFs. In both generators, the partonic processes are simulated using LO matrix elements, with the inclusion of initial- and final-state parton showers. Fragmentation into hadrons is performed using the Lund string model [26] as implemented in Jetset [22] in the case of Pythia, and a cluster model [27] in the case of Herwig.

These MC samples were used to correct the data to the hadron level, defined as those hadrons with lifetime $\tau \geq 10$ ps. For this purpose, the generated events were passed through the ZEUS detector- and trigger-simulation programs based on GEANT 3.13 [28]. They were reconstructed and analysed by the same program chain as the data. The jet search was performed using the energy measured in the CAL cells in the same way as for the data. The same jet algorithm was also applied to the final-state particles and to the partons available after the parton shower; the jets found in this way are referred to as hadronic and partonic jets, respectively.

5 Fixed-order calculations

The calculations of direct-photon processes used in this analysis are based on the program by Klasen, Kleinwort and Kramer [8]. The calculations use the phase-space-slicing method [29] with an invariant-mass cut to isolate the singular regions of the phase space. The number of flavours was set to five; the renormalisation, μ_R, and factorisation scales, μ_F, were set to $\mu_R = \mu_F = \mu = E_T^{\max}$, where $E_T^{\max}$ is the highest $E_T^{\rm jet}$; α_s was calculated at two loops using $\Lambda^{(5)}_{\overline{\rm MS}} = 220$ MeV, which corresponds to $\alpha_s(M_Z) = 0.1175$. The MRST99 [30] parameterisations of the parton distribution functions (PDFs) of the proton were used as defaults for the comparisons with the measured cross sections. These calculations are $\mathcal{O}(\alpha\alpha_s^2)$ and represent the lowest-order contribution to three-jet photoproduction. Full next-to-leading order corrections are not yet available for three-jet cross sections in photoproduction.

Since the measurements refer to jets of hadrons, whereas the calculations refer to partons, the predictions were corrected to the hadron level. The multiplicative correction factor, defined as the ratio of the cross section for jets of hadrons over that for jets of partons in direct-photon events, was estimated with the PYTHIA program. The normalised cross-section calculations changed typically by less than $\pm 5\%$ upon application of the parton-to-hadron corrections. Therefore, the effect of the parton-to-hadron corrections on the angular distributions is small.

The following theoretical uncertainties were considered:

- the uncertainty on the fixed-order calculations due to higher-order terms was estimated by varying μ between $E_T^{\rm jet}/2$ and $2E_T^{\rm jet}$;

- the uncertainty on the fixed-order calculations due to the uncertainties on the proton PDFs was estimated by using an alternative set of parameterisations, CTEQ5M1.

These uncertainties were added in quadrature and are shown as hatched bands in Fig. 4.

6 Results

Using the selected data sample, normalised three-jet differential cross sections were measured for $Q^2 < 1$ GeV^2, $0.2 < y < 0.85$ and $x_\gamma^{\rm obs} > 0.7$. The cross sections were determined for jets of $E_T^{\rm jet} > 14$ GeV and $-1 < \eta^{\rm jet} < 2.5$.

The cross-sections $(1/\sigma)(d\sigma/d\theta_H)$ and $(1/\sigma)(d\sigma/d\cos\alpha_{23})$ are presented in Figs. 2a and 2b, respectively. The measured cross section as a function of θ_H peaks around $\theta_H \sim 70^\circ$ and $(1/\sigma)(d\sigma/d\cos\alpha_{23})$ increases as $\cos\alpha_{23}$ increases. Figure 2c shows the normalised cross section as a function of $\cos\beta_{\rm KSW}$. This measured cross section shows a broad peak in the range of $\cos\beta_{\rm KSW}$ between -0.5 to 0.1.

The following experimental uncertainties were considered:

- the effect of the treatment of the parton shower and hadronisation was estimated by using the Herwig generator to evaluate the correction factors;
- the effect of the simulation of the trigger was evaluated by using an alternative trigger configuration, in both data and MC events;
- the effect of the uncertainty on y was estimated by varying $y_{\rm JB}$ by its uncertainty of $\pm 1\%$ in simulated events;
- the effect of the uncertainty on the parameterisations of the proton and photon PDFs was estimated by using alternative sets of PDFs in the MC simulation to calculate the correction factors;
- the effect of the uncertainty on the absolute energy scale of the calorimetric jets was estimated by varying $E_T^{\rm jet}$ by its uncertainty of $\pm 1\%$ in simulated events. The method used was the same as in earlier publications [15, 31].

These uncertainties were added in quadrature to the statistical uncertainty of the data and are shown as error bars in the figures. The uncertainty in the luminosity determination of 2.25% was not included.

Leading-logarithm parton-shower Monte Carlo calculations using Pythia and Herwig are compared to the data in Fig. 2. These calculations are the absolute predictions of the models including resolved and direct processes. The predictions of Pythia give a good description of the data, whereas those from Herwig give a poorer description. The predictions of Pythia for resolved and direct processes are also shown separately in Fig. 2 and found to be similar.

Fixed-order QCD direct-photon calculations, based on the SU(3) gauge symmetry group, separated into the color components according to Eq. 1, are compared to the data in Fig. 3. The predicted relative contributions are A: 13%, B: 10%, C: 45% and D: 32%. Therefore, the contribution from diagrams that involve the triple-gluon coupling amounts to 42% in SU(3). The component which contains the contribution from the triple-gluon vertex in quark-induced processes (Fig. 1B), σ_B, has a very different shape than the other components for the three angular variables considered here. The other components have distributions in $\beta_{\rm KSW}$ and θ_H that are similar and are best separated by the distribution of $\cos\alpha_{23}$. Thus, these variables are sensitive to the different color configurations and show a potential to extract the color factors. The full calculation, in which each contribution has been weighted according to the color factors predicted by SU(3), is compared to the data in Fig. 4. These calculations give a good description of the data for $\theta_H > 35°$, $\cos\alpha_{23} > -0.6$ and $-0.8 < \cos\beta_{\rm KSW} < 0.6$.

To illustrate the sensitivity of the measurements to the color factors, calculations based on different symmetry groups are also compared to the data in Fig. 4. In this figure, the color components have been combined in such way as to reproduce the color structure of a theory based on the non-abelian group SU(N) in the limit of large N ($C_F = (N^2 - 1)/2N, T_F = 1/2, C_A = N$), the abelian group U(1)^3 ($C_F = 1, T_F = 3, C_A = 0$) and, as an extreme choice, a calculation with $C_F = 0$, $T_F = 1/2$ and $C_A = 3$. The shapes of the distributions predicted by U(1)^3 are very similar to those by SU(3) due to the smallness of the component σ_B and the difficulty to distinguish the component σ_D. As can be seen from Fig. 4, the data clearly disfavour a theory in which $T_F/C_F \approx 0$ such as predicted by SU(N) in the limit of large N or $C_F = 0$.

7 Summary

Measurements of angular correlations in three-jet photoproduction have been made in *ep* collisions using 127 pb^{-1} of data collected with the ZEUS detector at HERA. The cross sections refer to jets identified with the longitudinally invariant k_T cluster algorithm in the inclusive mode and selected with $E_T^{\rm jet} > 14$ GeV and $-1 < \eta^{\rm jet} < 2.5$. The measurements were made in the kinematic region defined by $Q^2 \leq 1$ GeV^2, $0.2 < y < 0.85$ and $x_\gamma^{\rm obs} > 0.7$.

Normalised differential cross sections were measured as functions of θ_H, α_{23} and $\beta_{\rm KSW}$. Fixed-order ($\mathcal{O}(\alpha\alpha_s^2)$) calculations for three-jet photoproduction through direct-photon processes separated according to the color configurations were used to study the sensitivity of the angular distributions to the underlying gauge structure. The predicted distributions of θ_H, α_{23} and $\beta_{\rm KSW}$ distinguish well the contribution from the triple-gluon coupling in quark-induced processes. The variable α_{23} provides additional separation for the other contributions. The measurements are found to be consistent with the admixture of color configurations as predicted by SU(3). The data clearly disfavour a theory in which $T_F/C_F \approx 0$, as predicted by SU(N) in the limit of large N, or $C_F = 0$.

Acknowledgements

We would like to thank M. Fontannaz and M. Klasen for useful discussions.

References

[1] ALEPH Coll., R. Alemany et al., Phys. Lett. **B 284**, 151 (1992);
ALEPH Coll., R. Barate et al., Z. Phys. **C 76**, 1 (1997);
ALEPH Coll., A. Heister et al., Eur. Phys. J. **C 27**, 1 (2003);
DELPHI Coll., P. Abreu et al., Z. Phys. **C 59**, 357 (1993);
DELPHI Coll., P. Abreu et al., Phys. Lett. **B 414**, 401 (1997);
DELPHI Coll., P. Abreu et al., Phys. Lett. **B 449**, 383 (1999);
L3 Coll., B. Adeva et al., Phys. Lett. **B 248**, 227 (1990);
OPAL Coll., M.Z. Akrawy et al., Z. Phys. **C 49**, 49 (1991);
OPAL Coll., R. Akers et al., Z. Phys. **C 65**, 367 (1995);
OPAL Coll., G. Abbiendi et al., Eur. Phys. J. **C 20**, 601 (2001).

[2] DELPHI Coll., P. Abreu et al., Phys. Lett. **B 255**, 466 (1991).

[3] C.H. Llewellyn Smith, Phys. Lett. **B 79**, 83 (1978);
I. Kang and C.H. Llewellyn Smith, Nucl. Phys. **B 166**, 413 (1980);
J.F. Owens, Phys. Rev. **D 21**, 54 (1980);
M. Fontannaz, A. Mantrach and D. Schiff, Z. Phys. **C 6**, 241 (1980).

[4] W.J. Stirling and Z. Kunszt, *Proc. HERA Workshop*, R.D. Peccei (ed.), Vol. 2, p. 331. DESY, Hamburg, Germany (1987);
M. Drees and F. Halzen, Phys. Rev. Lett. **61**, 275 (1988);
M. Drees and R.M. Godbole, Phys. Rev. Lett. **61**, 682 (1988);
M. Drees and R.M. Godbole, Phys. Rev. **D 39**, 169 (1989);
H. Baer, J. Ohnemus and J.F. Owens, Z. Phys. **C 42**, 657 (1989);
H. Baer, J. Ohnemus and J.F. Owens, Phys. Rev. **D 40**, 2844 (1989).

[5] R. Muñoz-Tapia and W.J. Stirling, Phys. Rev. **D 52**, 3894 (1995).

[6] J.G. Körner, G. Schierholz and J. Willrodt, Nucl. Phys. **B 185**, 365 (1981).

[7] ZEUS Coll., J. Breitweg et al., Phys. Lett. **B 443**, 394 (1998).

[8] M. Klasen, T. Kleinwort and G. Kramer, Eur. Phys. J. Direct **C 1**, 1 (1998).

[9] P. Aurenche et al., Nucl. Phys. **B 286**, 553 (1987).

[10] ZEUS Coll., M. Derrick et al., Phys. Lett. **B 293**, 465 (1992).

[11] ZEUS Coll., U. Holm (ed.), *The ZEUS Detector*. Status Report (unpublished), DESY (1993), available on `http://www-zeus.desy.de/bluebook/bluebook.html`.

[12] N. Harnew et al., Nucl. Inst. Meth. **A 279**, 290 (1989);
B. Foster et al., Nucl. Phys. Proc. Suppl. **B 32**, 181 (1993);
B. Foster et al., Nucl. Inst. Meth. **A 338**, 254 (1994).

[13] M. Derrick et al., Nucl. Inst. Meth. **A 309**, 77 (1991);
A. Andresen et al., Nucl. Inst. Meth. **A 309**, 101 (1991);
A. Caldwell et al., Nucl. Inst. Meth. **A 321**, 356 (1992);
A. Bernstein et al., Nucl. Inst. Meth. **A 336**, 23 (1993).

[14] J. Andruszków et al., Preprint DESY-92-066, DESY, 1992;
ZEUS Coll., M. Derrick et al., Z. Phys. **C 63**, 391 (1994);
J. Andruszków et al., Acta Phys. Pol. **B 32**, 2025 (2001);
W.H. Smith, K. Tokushuku and L.W. Wiggers, *Proc. Computing in High-Energy Physics (CHEP), Annecy, France, Sept. 1992*, C. Verkerk and W. Wojcik (eds.), p. 222. CERN, Geneva, Switzerland (1992). Also in preprint DESY 92-150B.

[15] ZEUS Coll., S. Chekanov et al., Phys. Lett. **B 560**, 7 (2003).

[16] S. Catani et al., Nucl. Phys. **B 406**, 187 (1993).

[17] S.D. Ellis and D.E. Soper, Phys. Rev. **D 48**, 3160 (1993).

[18] J.E. Huth et al., *Research Directions for the Decade. Proc. of Summer Study on High Energy Physics, 1990*, E.L. Berger (ed.), p. 134. World Scientific (1992). Also in preprint FERMILAB-CONF-90-249-E.

[19] H. Abramowicz, A. Caldwell and R. Sinkus, Nucl. Inst. Meth. **A 365**, 508 (1995);
R. Sinkus and T. Voss, Nucl. Inst. Meth. **A 391**, 360 (1997).

[20] ZEUS Coll., M. Derrick et al., Phys. Lett. **B 322**, 287 (1994).

[21] F. Jacquet and A. Blondel, *Proc. of the Study for an ep Facility for Europe*, U. Amaldi (ed.), p. 391. Hamburg, Germany (1979). Also in preprint DESY 79/48.

[22] T. Sjöstrand, Comp. Phys. Comm. **82**, 74 (1994);
T. Sjöstrand et al., Comp. Phys. Comm. **135**, 238 (2001).

[23] G. Marchesini et al., Comp. Phys. Comm. **67**, 465 (1992);
G. Corcella et al., JHEP **0101**, 010 (2001).

[24] M. Glück, E. Reya and A. Vogt, Phys. Rev. **D 45**, 3986 (1992);
M. Glück, E. Reya and A. Vogt, Phys. Rev. **D 46**, 1973 (1992).

[25] H.L. Lai et al., Eur. Phys. J. **C 12**, 375 (2000).

[26] B. Andersson et al., Phys. Rep. **97**, 31 (1983);
T. Sjöstrand, Comp. Phys. Comm. **39**, 347 (1986);
T. Sjöstrand and M. Bengtsson, Comp. Phys. Comm. **43**, 367 (1987).

[27] B.R. Webber, Nucl. Phys. **B 238**, 492 (1984).

[28] R. Brun et al., GEANT3, Technical Report CERN-DD/EE/84-1, CERN, 1987.

[29] G. Kramer, *Theory of Jets in Electron-Positron Annihilation*. Springer, Berlin, (1984).

[30] A.D. Martin et al., Eur. Phys. J. **C 4**, 463 (1998);
A.D. Martin et al., Eur. Phys. J. **C 14**, 133 (2000).

[31] ZEUS Coll., S. Chekanov et al., Eur. Phys. J. **C 23**, 615 (2002);
ZEUS Coll., S. Chekanov et al., Phys. Lett. **B 531**, 9 (2002);
M. Wing (on behalf of the ZEUS Coll.), *Proc. of the 10th International Conference on Calorimetry in High Energy Physics*, R. Zhu (ed.), p. 767. Pasadena, USA (2002). Also in preprint hep-ex/0206036.

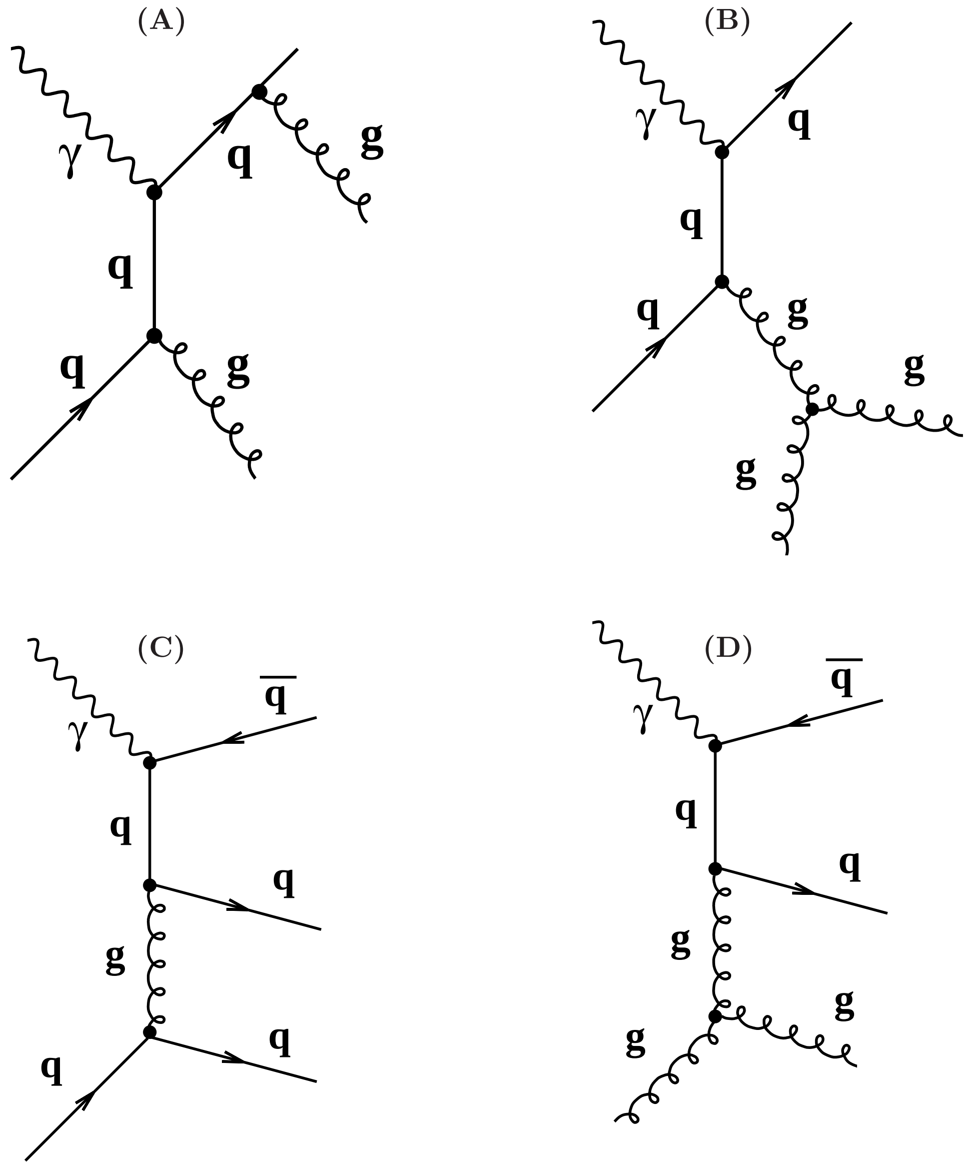

Figure 1: *Examples of diagrams for the photoproduction of three-jet events through direct-photon processes in each color configuration: (A) double-gluon bremsstrahlung from a quark line, C_F^2; (B) the splitting of a virtual gluon into a pair of final-state gluons, $C_F C_A$; (C) the production of a $q\bar{q}$ pair through the exchange of a virtual gluon emitted by an incoming quark, $C_F T_F$; (D) the production of a $q\bar{q}$ pair through the exchange of a virtual gluon arising from the splitting of an incoming gluon, $T_F C_A$.*

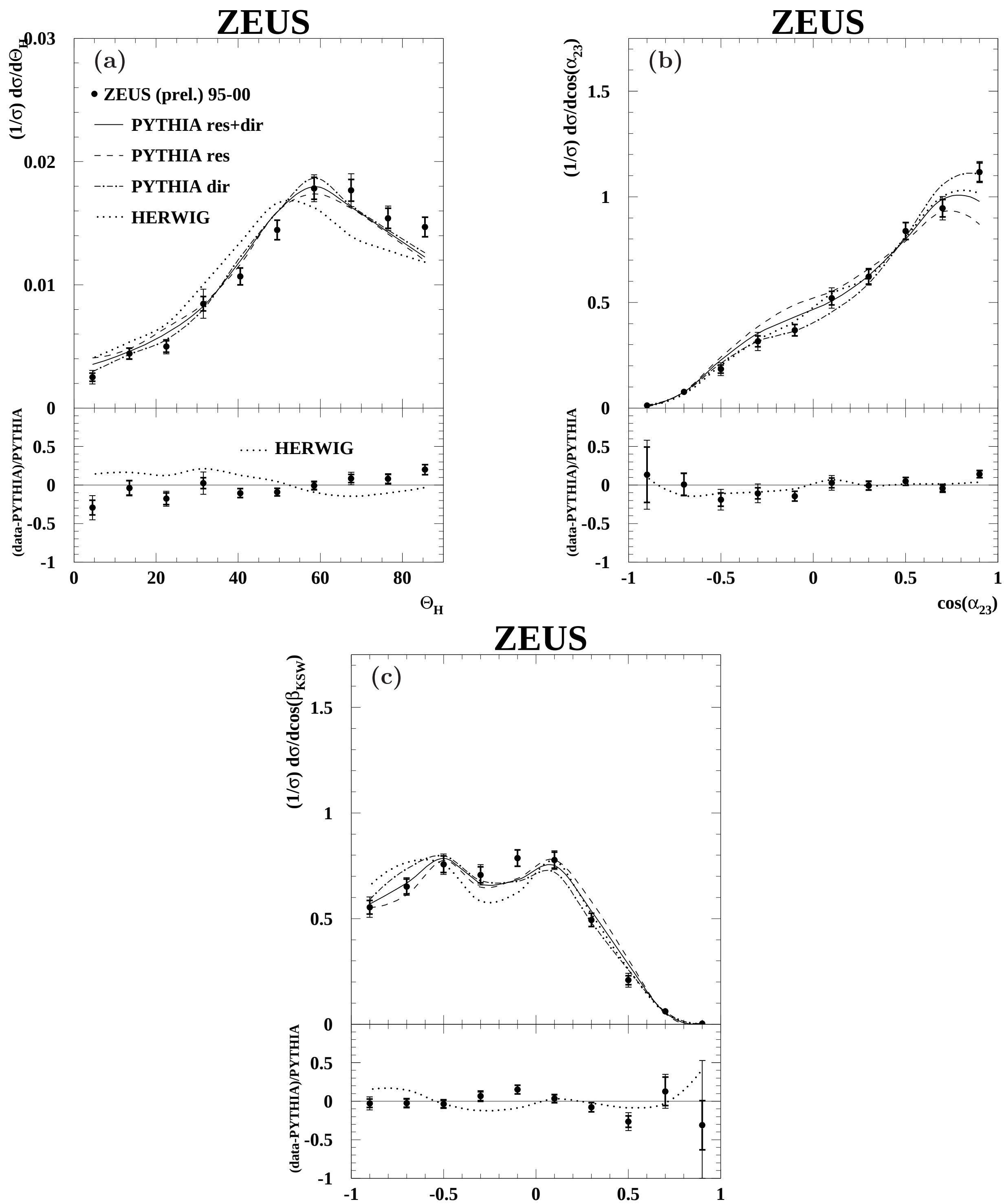

Figure 2: *Normalised differential ep cross sections for three-jet photoproduction integrated over* $E_T^{\rm jet} > 14$ *GeV and* $-1 < \eta^{\rm jet} < 2.5$ *in the kinematic region defined by* $Q^2 < 1$ *GeV*^{2}, $0.2 < y < 0.85$ *and* $x_\gamma^{\rm obs} > 0.7$ *as functions of (a)* θ_H*, (b)* $\cos\alpha_{23}$ *and (c)* $\cos\beta_{\rm KSW}$*. The thick error bars represent the statistical uncertainties of the data, and the thin error bars show the statistical and systematic uncertainties added in quadrature. For comparison, the predictions of leading-logarithm parton-shower Monte Carlo models of* PYTHIA *(resolved: dashed lines, direct: dot-dashed lines and resolved plus direct: solid lines) and* HERWIG *(resolved plus direct: dotted lines) are included. The lower part of the figures displays the fractional difference between the measured cross section and the prediction of* PYTHIA *for resolved plus direct processes (black dots); the fractional difference between the predictions of* HERWIG *and* PYTHIA *is also shown (dotted lines).*

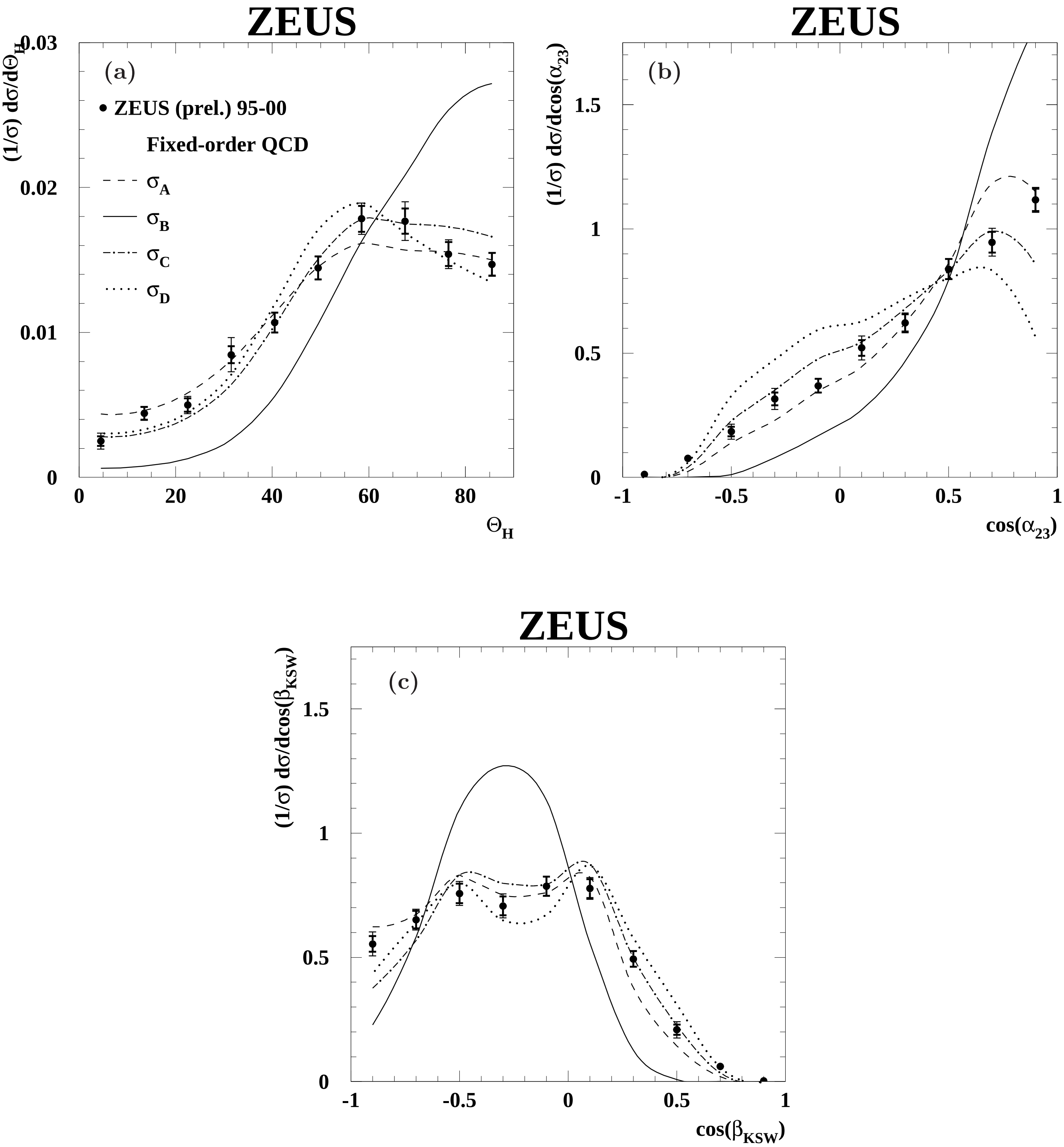

Figure 3: *Normalised differential ep cross sections for three-jet photoproduction integrated over* $E_T^{\rm jet} > 14$ *GeV and* $-1 < \eta^{\rm jet} < 2.5$ *in the kinematic region defined by* $Q^2 < 1$ *GeV*^{2}, $0.2 < y < 0.85$ *and* $x_\gamma^{\rm obs} > 0.7$ *as functions of (a)* θ_H, *(b)* $\cos\alpha_{23}$ *and (c)* $\cos\beta_{\rm KSW}$. *Other details as in the caption to Fig. 2. For comparison, the color components of the* $\mathcal{O}(\alpha\alpha_s^2)$ *QCD calculations [8] for direct-photon processes (see text) are included.*

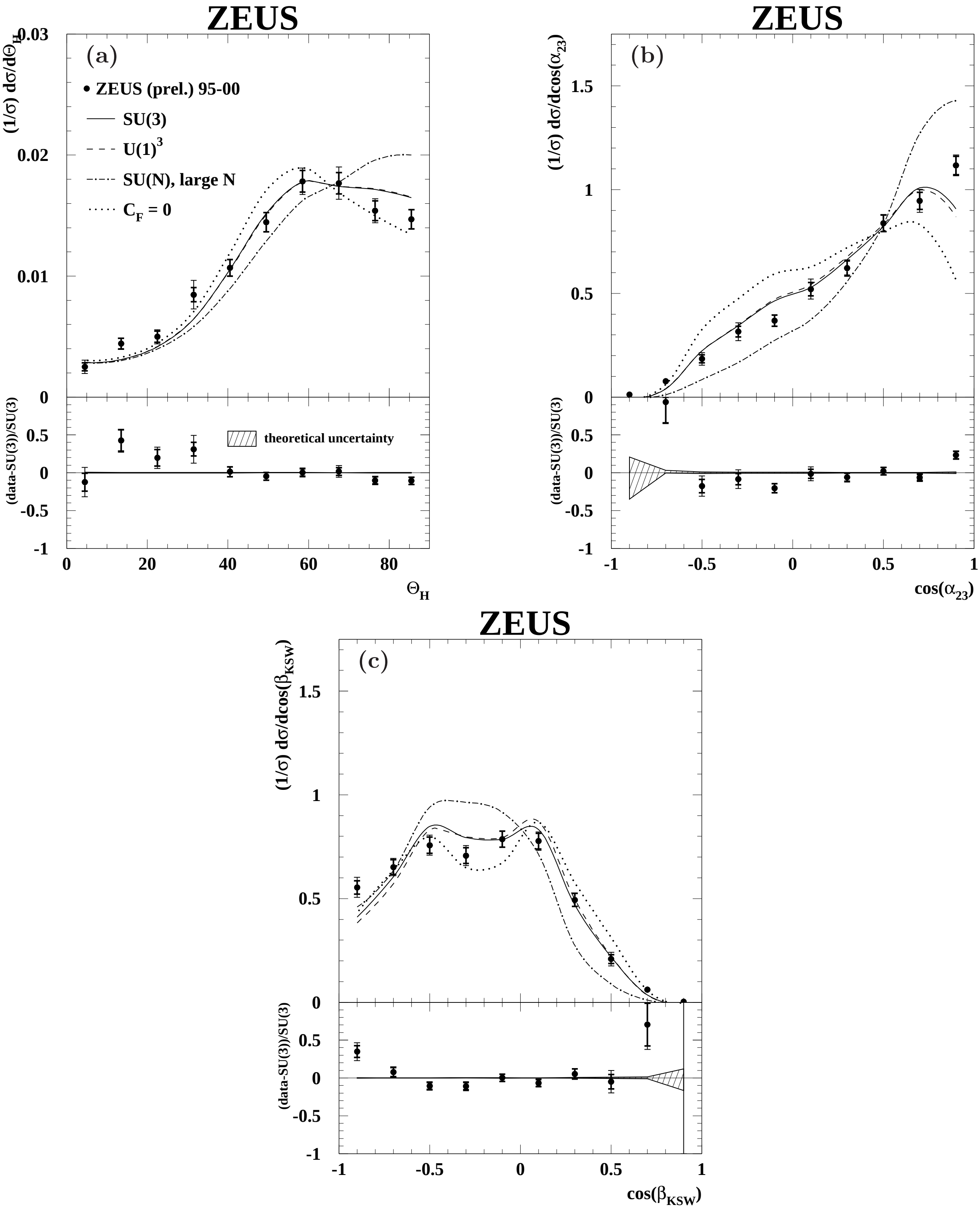

Figure 4: *Normalised differential ep cross sections for three-jet photoproduction integrated over $E_T^{\rm jet} > 14$ GeV and $-1 < \eta^{\rm jet} < 2.5$ in the kinematic region defined by $Q^2 < 1$ GeV^2, $0.2 < y < 0.85$ and $x_\gamma^{\rm obs} > 0.7$ as functions of (a) θ_H, (b) $\cos\alpha_{23}$ and (c) $\cos\beta_{\rm KSW}$. Other details as in the caption to Fig. 2. For comparison, the the $\mathcal{O}(\alpha\alpha_s^2)$ calculations [8] for direct-photon processes (see text) based on SU(3) (solid lines), U(1)^3 (dashed lines), SU(N) in the limit of large N (dot-dashed lines) and $C_F = 0$ (dotted lines) are included. The lower part of the figures displays the fractional difference between the measured cross section and the calculation based on SU(3); the hatched band shows the uncertainty of the calculation.*